Infrared Spectroscopy of Human Apolipoprotein Fragments in SDS/D_2O: Relative Lipid-Binding Affinities and a Novel Amide I Assignment†

R. A. Shaw,*,‡ G. W. Buchko,§,|| G. Wang,§ A. Rozek,§ W. D. Treleaven,§,⊥ H. H. Mantsch,‡ and R. J. Cushley§

Institute for Biodiagnostics, National Research Council of Canada, 435 Ellice Avenue, Winnipeg, Manitoba, Canada R3B 1Y6, and Institute of Molecular Biology and Biochemistry, Simon Fraser University, Burnaby, British Columbia, Canada V5A 1S6

Received March 11, 1997; Revised Manuscript Received June 18, 1997⊗

ABSTRACT: Infrared absorption spectra are reported for six apolipoprotein fragments in SDS/D_2O. Five of the peptides correspond to proposed lipid-binding domains of human apolipoproteins [apoC-I(7−24), apoC-I(35−53), apoA-II(18−30)+, apoA-I(166−185), apoE(267−289)], and the sixth is the *de novo* lipid associating peptide LAP-20. The amide I infrared absorption patterns are generally consistent with predominantly helical structures (as determined previously by NMR spectroscopy and distance geometry calculations) and further suggest that apoA-I(166−185) and apoE(267−289) are bound to SDS relatively weakly in comparison to the other four peptides. The latter conclusion is also supported by the temperature dependence of the infrared spectra, as increasing temperature promotes a distinct increase in random coil structure only for apoA-I(166−185) and apoE(267−289). In addition to features readily ascribed to helices, the infrared spectra of all the peptides show absorptions in the spectral region 1630−1635 cm^{-1} that is usually associated with β-structure, a motif that is clearly absent from the NMR-derived structures. Parallel difficulties also arose in the analyses of the circular dichroism spectra. We suggest that both the low-frequency infrared absorptions and the ambiguities in interpreting the CD spectra may be due to unusual structures at the peptide C-termini, involving C═O groups that form hydrogen bonds simultaneously either with two solvent molecules or with donors from the backbone (NH) and the solvent (OH). Analogous absorptions may be a general feature of solvent-exposed helices, which suggests a need for caution in assigning amide I bands below 1640 cm^{-1}.

Plasma lipids are transported via the circulatory system of animals in specialized lipoprotein complexes. These complexes consist of a hydrophobic lipid core of cholesterol esters and/or triglycerides surrounded by a surface monolayer of cholesterol, phospholipids, and apolipoproteins (Shen et al., 1977; Assman & Brewer, 1974; Segrest et al., 1974). In addition to imparting solubility to otherwise insoluble lipids and providing structural stabilization of the lipoprotein particles, apolipoproteins modulate lipoprotein metabolism and serve as ligands for receptor-mediated lipoprotein endocytosis and as ligands for cell surface lipoprotein receptors (Ryan, 1996; Mahley, 1988). Transformation of HDL (high-density lipoprotein) provides the basis for the process of reverse cholesterol transport, a process by which cholesterol is transported from the peripheral tissues to the liver for excretion from the body (Atkinson & Small, 1986; Dolphin et al., 1985). The fact that HDL levels are inversely correlated with the risk of atherosclerosis (Miller & Miller, 1975) has led to strong interest in the structure and function of lipoproteins and their constituents.

The major proteins in mature HDL are apoA-I (∼60−75%) and apoA-II (∼20−30%), with small amounts of apoCs (C-I, C-II, C-III) and apoE (Lusis, 1988). A prominent feature of the exchangeable plasma lipoproteins is the repeating amino acid motif of 11 or 22 residues which may adopt an amphipathic helical structure when associated with lipid. It is postulated that such amphipathic regions, characterized by polar (hydrophilic) and nonpolar (lipophilic) amino acid residues aligned on opposing faces of the long axis of an α-helix, stabilize lipoproteins through concomitant interaction with lipid and the aqueous milieu (Segrest et al., 1994). Both experimental and predictive methods have been used to identify apolipoprotein lipid-binding domains, with many of these sequences having been isolated or synthesized in order to further understand the nature of the protein/lipid interactions. Using deuterated sodium dodecyl sulfate to model the lipoprotein environment and distance geometry/simulated annealing methods based on NOE-derived distance restraints, it has been shown that synthetic peptides containing proposed lipid-binding domains of apoA-I, apoA-II, apoC-I, and apoE do indeed adopt an amphipathic helical structure when associated with lipid (Rozek et al., 1995; Buchko et al., 1996a,b; Wang et al., 1996a,b). The same is true for the synthetic lipid-associating peptide LAP-20 (Buchko et al., 1996a), which activates lecithin−cholesterol acyltransferase (LCAT) despite its lack of sequence homology to apoA-I, the primary *in vivo* activator of LCAT (Pownall et al., 1980).

Infrared (IR) spectroscopy of the amide I (backbone C═O stretching) absorptions has proven to be valuable as a probe of protein and peptide secondary structures both in solution

† Issued as NRCC Publication No. 34783.

* Correspondence should be addressed to this author at the National Research Council of Canada, Institute for Biodiagnostics, 435 Ellice Ave., Winnipeg, Manitoba, Canada R3B 1Y6. Telephone: (204) 984-4626. FAX: (204) 984-5472. E-mail: shaw@ibd.nrc.ca.

‡ National Research Council of Canada.

§ Simon Fraser University.

|| Present address: Environmental Molecular Sciences Laboratory, Pacific Northwest National Laboratories, Richland, WA 99352.

⊥ Present address: College of Basic Science, Louisiana State University, Baton Rouge, LA 70803.

⊗ Abstract published in *Advance ACS Abstracts,* November 1, 1997.

S0006-2960(97)00558-8 CCC: $14.00

Table 1: Primary Structures

apoA-I(166−185)	YSDELRQRLAARLEALKENG
apoA-II(18−30)+[a]	VTDYGKDLMEKVKEWLNS
apoC-I(7−24)	ALDKLKEFGNTLEDKARE
apoC-I(35−53)	SAKMREWFSETFQKVKEKL
apoE(267−289)	PLVEDMQRQWAGLVEKVQAAVGT
LAP-20[b]	VSSLLSSLKEYWSSLKESFS

[a] ApoA-II residues 18−30 with a five-residue amphipathic motif, EWLNS, added to the C-terminus. [b] A *de novo* peptide which closely mimics apoA-I in its ability to activate LCAT (Pownall et al., 1980).

and in membranes or membrane mimetic environments (Byler & Susi, 1986; Surewicz & Mantsch, 1988; Surewicz et al., 1993). The IR method is particularly well suited for comparing and contrasting secondary structures in groups of proteins or peptides that share common structural features. The proposed lipid-binding domains of the apolipoproteins are attractive in this respect, as they are generally similar in size (between 18 and 23 residues) and all are believed to adopt amphipathic helical structures upon interaction with lipid.

We have therefore carried out an IR spectroscopic study of the interactions with a lipid mimetic (SDS/D_2O) environment for five peptides, apoC-I(7−24), apoC-I(35−53), apoA-II(18−30)+, apoA-I(166−185), and apoE(267−289), each of which represents a lipid-binding domain of the parent apolipoprotein, and for the *de novo* peptide LAP-20. The amide I IR absorptions were first partially assigned with reference to detailed NMR-based solution structures previously reported for each peptide in SDS/D_2O (Rozek et al., 1995; Buchko et al., 1996a,b; Wang et al., 1996a,b). IR absorptions below 1640 cm^{-1} appeared in all of the IR absorption spectra; several of the experiments reported here were designed specifically to assign these absorptions and hence to completely reconcile the IR spectra with the NMR-derived structures. Certain features of the IR spectra were found to correlate with previous model-based estimates of lipid-binding affinity. We suggest that the IR spectra, and particularly their temperature dependence, may serve as sensitive indicators of relative peptide/lipid-binding affinities.

MATERIALS AND METHODS

Peptides were synthesized by Dr. Ian Clark-Lewis (University of British Columbia) using solid-phase methods (Clark-Lewis et al., 1986). The primary structures are listed in Table 1. While details of the CD and NMR spectroscopy and NMR structure calculations have been reported previously (Rozek et al., 1995; Buchko et al., 1996a,b; Wang et al., 1996a,b), a summary of the major features is included below.

Infrared Spectroscopy. IR spectra (512 scans) were recorded at a nominal resolution of 2 cm^{-1}, using a Digilab FTS-40A spectrometer equipped with an MCT liquid nitrogen-cooled detector. For peptide solutions in SDS/D_2O, the peptide concentrations were typically 20 mg/mL at a peptide:SDS molar ratio of 1:40 and at a pH between 3.8 and 6 (the possibility of self-association at these concentrations is ruled out by the NMR measurements, in particular by the absence of the NOE's characteristic of intermolecular hydrogen bond formation). The temperature dependence was investigated by recording IR spectra of these solutions at 5 °C intervals from 15 °C to 80 °C. IR absorption spectra were also acquired for 10 mg/mL solutions of apoC-I(7−24) in 75% and 50% mixtures of trifluoroethanol-d_3 with D_2O. All spectra were obtained by placing ~10 μL of the sample solution between two CaF_2 windows separated by a 50 μm Teflon spacer and mounting this 'sandwich' in a demountable liquid cell (Harrick) in the IR spectrometer. Solvent absorptions were compensated by iterative subtraction of a spectrum of the solvent. Absorptions due to atmospheric water vapor were minimized by purging the sample compartment with dry air; residual H_2O absorptions were then eliminated via interactive subtraction of a water vapor spectrum. Spectra were then deconvolved to resolve subcomponent spectral features and derivatized when necessary to resolve the positions of closely spaced absorptions. Deconvolved spectra were curve-fitted using absorption positions measured for the deconvolved and/or derivatized spectra. Spectral deconvolution, derivation, and curve-fitting were performed using software developed at the National Research Council. In order to assess (retrospectively) its possible influence upon the peptide secondary structures, trifluoroacetate was removed from one sample [apoC-I(7−24)] by lyophilizing 3 mg of the peptide from solution in 4 mL of DCl/D_2O (pD = 2).

Circular Dichroism. CD spectra were measured in the presence of a 40-fold molar excess of SDS (aqueous solution) using a Jasco J710 spectropolarimeter, calibrated using ammonium *d*-(+)-camphorsulfonate. The measurements were performed on a 0.1−0.7 mM sample in a quartz cell of 0.1 or 0.2 cm path length, at pH between 4.8 and 6.6. The cell was held at constant temperature using a circulating water bath (Neslab RTE-110). Spectra are reported as the average of two scans, recorded with a bandwidth of 0.5 nm, time constant of 0.25 s, and scan rate of 10−20 nm/min. Following base line correction and noise reduction, the observed ellipticities were converted to mean residue ellipticities, $[\theta]$, in units of degrees centimeter squared per decimole. Secondary structures were estimated using convex constraint analysis (Perczel et al., 1992).

NMR Spectroscopy. Five millimolar samples [2.9 mM for apoE(267−289)] were prepared in 90% H_2O/10% D_2O by dissolving the peptides in a 40-fold molar excess of SDS-d_{25}. The pH was adjusted to between 4.6 and 6.0 with the addition of 0.1 M NaOH (pH meter readings uncorrected for the deuterium isotope effect).

Standard phase sensitive (TPPI) (Redfield & Kunz, 1975) two-dimensional NOESY (Jeener et al., 1979), TOCSY (Braunschweiler & Ernst, 1983; Bax & Davis, 1985), and DQF-COSY spectra were recorded on a Bruker AMX spectrometer operating at a proton frequency of 600.13 MHz. The H_2O signal was suppressed in the TOCSY and NOESY experiments using the Watergate technique (Piotto et al., 1992) which employed the 3-9-19 pulse sequence (Sklenar et al., 1993). Prior to Fourier transformation, the data were zero-filled to generate a 2K × 2K matrix and apodized by shifted sine-bell or quadratic sine-bell window functions in both dimensions. Base line corrections (fifth order polynomial) were applied in both dimensions to all processed spectra. Chemical shifts were referenced to external sodium 4,4-dimethyl-4-silapentane-1-sulfonate (DSS, 0.0 ppm).

Structure Calculations. Three-dimensional structures were calculated from the NOE distance restraints (FELIX) using the distance geometry program (DGII) of Insight II (MSI).

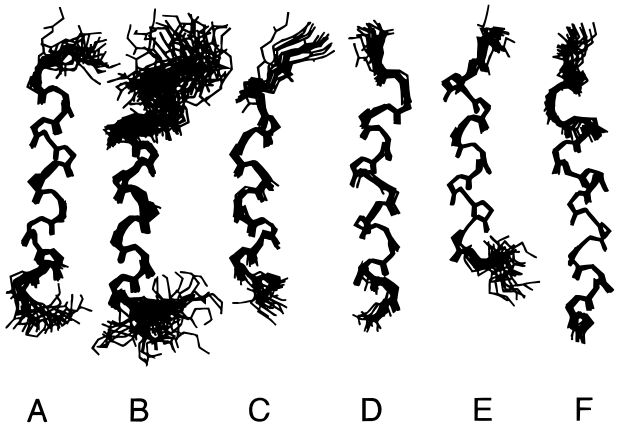

FIGURE 1: Conformational ensembles of peptide backbones calculated from NOE-based distance restraints using distance geometry simulated annealing methods described by Rozek et al. (1995). (A) ApoA-I(166−185), 19 structures displayed out of 20 calculated; (B) apoE(267−289), 37 out of 50; (C) apoA-II(18−30)+, 15 out of 20; (D) apoC-I(35−53), 20 out of 20; (E) apoC-I(7−24), 20 out of 20; (F) LAP-20, 17 out of 20. The N-terminal corresponds to the upper end of each plotted structure.

Peak volumes were classified into strong (∼1.80−3.00 Å), medium (∼2.51−4.00 Å), and weak (∼3.51−5.50 Å) ranges. The upper bound of restraints involving nonresolvable methylene or methyl protons was adjusted by the addition of 1.0 and 1.5 Å, respectively, using the NMR-Refine module of InsightII. Nonresolvable methyl groups were adjusted by the addition of 2.4 Å to the upper bound. The distance geometry calculations consisted of three steps; smoothing, embedding, and optimization, the latter step based upon simulated annealing and energy minimization of the annealed structures with a conjugated gradient (Havel, 1991). The CVFF force field was used with the upper and lower force constant set at 10−32 kcal/(mol·Å^2) and the maximum force constant set at 100 kcal/(mol·Å^2). Simulated annealing was performed by first "cooking" to 200 K and then slowly "cooling" to 0 K over 10 000 steps of 0.2 ps duration. Following the generation of 10−20 distance geometry/simulated annealing derived structures, the distance restraints were either widened or eliminated to reflect uncertainty in the distance classification or the integration of overlapping cross-peaks. The process was repeated until no distance violation greater than 0.1 Å was observed. The fail level was then set above the optimization error to effect the execution of a conjugated gradient minimization of a final set of 20−50 structures. From the final set of structures, a subset with the best convergence (displayed in Figure 1) was selected for structure analysis.

RESULTS

Backbone ensembles of the NMR-derived structures in SDS/D_2O are illustrated for each peptide in Figure 1. The interested reader is referred to the original reports for details (Rozek et al., 1995; Buchko et al., 1996a,b; Wang et al., 1996a,b). They are reproduced here to illustrate the main structural features; the core residues adopt a well-defined helical structure while the terminal residues are 'frayed'. The overall flexibility may be estimated from the RMSD of the ensemble of structures to their mean structure. (The overall backbone RMSD's are summarized in Table 2, together with the corresponding averages for sections to either side of the peptide midpoint.) Although a variety of factors may contribute to the overall values, it is generally true that a lower RMSD implies a more rigid structure; for example, the severe fraying at the N-terminal of apoE(267−289) that is evident in Figure 1 translates to the largest overall RMSD at the N-terminal. In this instance, the disorder implied by the relatively large RMSD may relate to relatively loose association with SDS.

Table 2: RMSD's in NMR-Derived Geometries

	N-terminal[a]	C-terminal[a]	overall[b]
apoA-I(166−185)	0.44 (167−175)	0.21 (176−182)	0.83
apoA-II(18−30)+	0.26 (19−26)	0.16 (27−33)	0.54
apoC-I(7−24)	0.20 (8−15)	0.18 (16−21)	0.73
apoC-I(35−53)	0.27 (36−43)	0.13 (44−51)	0.48
apoE(267−289)	0.74 (268−275)	0.34 (276−286)	0.79
LAP-20	0.32 (2−9)	0.06 (10−18)	0.41

[a] Backbone RMSD's (Å) calculated for the residues in parentheses. Derived from structures reported by Rozek et al. (1995), Buchko et al. (1996a,b), and Wang et al. (1996a,b). [b] RMSD for all backbone atoms.

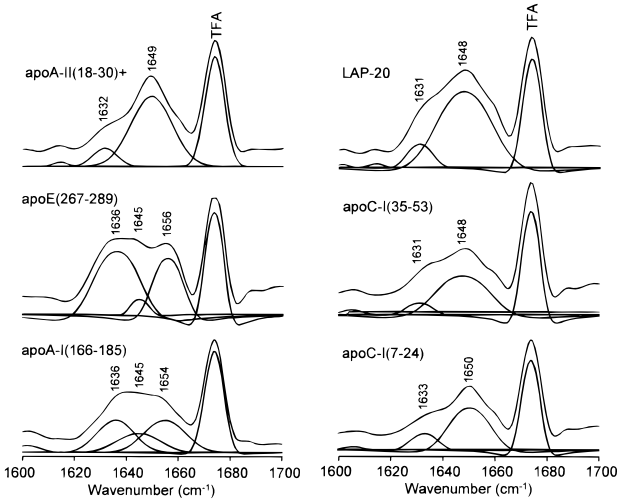

FIGURE 2: Infrared absorption spectra in the amide I region for apoA-I(166−185), apoA-II(18−30)+, apoE(267−289), apoC-I(7−24), apoC-I(35−53), and LAP-20 in SDS/D_2O solution (25 °C, molar peptide:SDS ratio = 1:40), autoscaled and offset for clarity. All spectra were deconvolved (half-bandwidth = 16 cm^{-1}, band narrowing factor = 2) and least-squares curve-fitted to yield the component curves plotted below each spectrum. The prominent absorption at 1673 cm^{-1} in all spectra is due to trifluoroacetate (TFA) used in the purification of the peptides. The shoulder at *ca.* 1658 cm^{-1} (and the weak feature at *ca.* 1688 cm^{-1}) in each spectrum is a minor artifact that arises due to the relatively narrow TFA absorption being 'overdeconvolved' using the parameters that are optimal for resolving the amide I bands.

Figure 2 displays the deconvolved IR absorption spectra for the six peptides in the amide I region, and the component bands derived via curve-fitting. Vibrational assignments and relative absorption intensities for the amide I absorptions are summarized in Table 3 (the weak bands observed below 1620 cm^{-1} are side chain absorptions, and the band observed at 1673 cm^{-1} is due to trifluoroacetate used in the purification of the peptides). The dominant absorptions observed in all spectra at 1648−1656 cm^{-1} correspond to α-helical regions (Surewicz & Mantsch, 1988; Byler & Susi, 1986). Consistent with the relatively large RMSD's in the NMR-derived structures, the IR spectra for apoE(267−289) and apoA-I(166−185) are the only two that include distinct bands corresponding to random coil structure (1645 cm^{-1}). Each of the six spectra also includes a low-frequency component at 1631−1636 cm^{-1}.

Table 3: Amide I Infrared Absorptions

	helix[a]	random coil	other
apoA-I(166−185)	1654 (40)	1645 (20)	1636 (40)
apoA-II(18−30)+	1649 (80)		1632 (20)
apoC-I(7−24)	1650 (80)		1633 (20)
apoC-I(35−53)	1648 (80)		1631 (20)
apoE(267−289)	1656 (40)	1645 (20)	1636 (40)
LAP-20	1648 (75)		1631 (25)

[a] Absorption frequency (in cm^{-1}) and approximate relative intensity as a percentage of overall amide I integrated area (in parentheses).

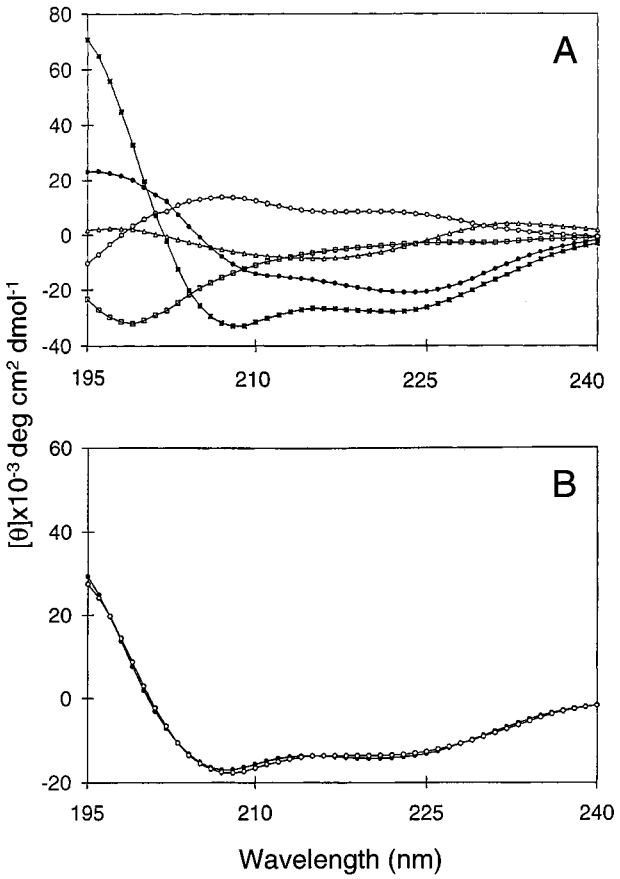

FIGURE 3: (A) Pure component curves for 0.1 mM apoA-I(166−185) in SDS (1:40 peptide:SDS mol/mol) at 25 °C, obtained from a five-component convex constraint analysis of the CD spectrum. (B) Experimentally determined CD curve for apoA-I(166−185) in SDS (open circles) and the superposition of pure component CD curves (closed circles).

The circular dichroism spectrum of apoA-I(166−185) in SDS/D_2O is plotted in Figure 3, which also shows the five components generated by the convex constraint analysis (Perczel et al., 1992) and the fit of calculated to experimental spectrum (Figure 3B). This analysis indicates predominantly helical structures (Table 4) together with regions of random coil structure for all six peptides and, particularly for apoE-(267−289) and apoA-I(166−185), contributions from components attributed to β-pleats and β- and γ-turns labeled as 'other' in Table 4. In the absence of SDS, the amount of helix calculated by CCA ranged from 2 to 15% with the remainder random coil (Rozek et al., 1995; Buchko et al., 1996a,b; Wang et al., 1996a,b).

The thermal stability of the secondary structures was evaluated by measuring IR spectra in SDS/D_2O at 5 °C intervals between 15 and 80 °C (Figure 4), and the spectra for apoA-I(166−185) were curve-fitted in order to discern

Table 4: Percent Secondary Structures in SDS/D_2O As Determined by Convex Constraint Analysis of the CD Spectra; All Samples Are at a 1:40 Peptide:SDS Molar Ratio

	helix	random coil	other[a]
apoA-I(166−185)[b]	50	29	21
apoA-II(18−30)+[c]	55	39	6
apoC-I(7−24)[d]	64	36	0
apoC-I(35−53)[e]	54	32	14
apoE(267−289)[f]	50	17	33
LAP-20[g]	64	32	4

[a] Components originally attributed to β-sheet and γ- and β-turns (Perczel et al., 1992). [b] Wang et al. (1996b). [c] Buchko et al. (1996b). [d,e] Rozek et al. (1995). [f] Wang et al. (1996a). [g] Buchko et al. (1996a).

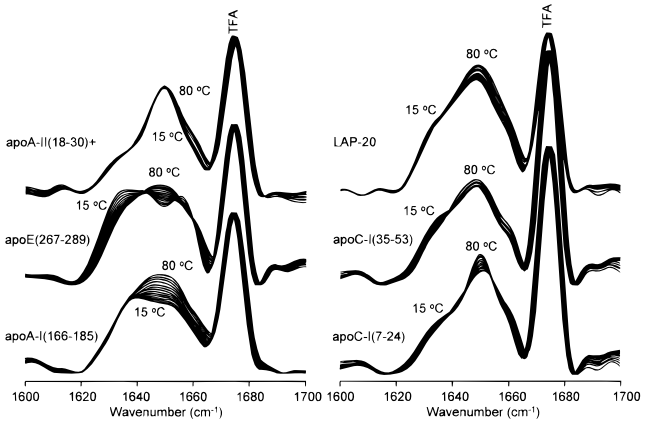

FIGURE 4: Infrared spectra measured for apoA-I(166−185), apoA-II(18−30)+, apoE(267−289), apoC-I(7−24), apoC-I(35−53), and LAP-20 in SDS/D_2O over the temperature range of 15−80 °C in increments of 5 °C. The spectra are scaled such that the 1673 cm^{-1} absorption of trifluoroacetate (TFA) is of equal height in all spectra, and deconvolved (bandwidth = 16 cm^{-1}, band narrowing factor = 2). See legend to Figure 2 for further details.

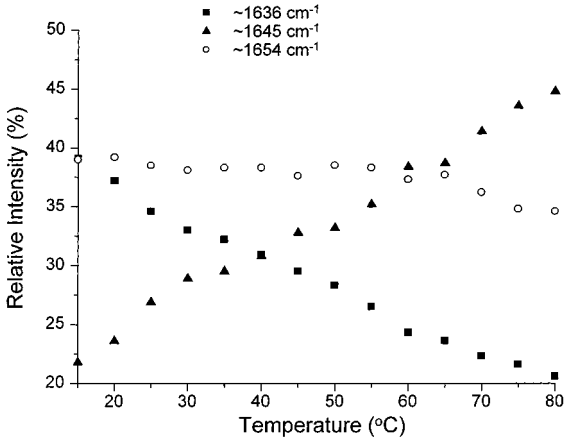

FIGURE 5: Relative intensities (percent) of the three curve-fitted components of the apoA-I(166−185) amide I infrared absorption profile as a function of temperature. The positions for these components also changed with increasing temperature, from 1636, 1645, and 1654 cm^{-1} at 15 °C to 1635, 1647, and 1659 cm^{-1}, respectively, at 80 °C.

trends in the subcomponent intensities (Figure 5). The stability of the apoA-I(166−185) helical structure in SDS/D_2O was further assessed by collecting CD spectra both at 37 and at 87 °C. Convex constraint analyses of the CD spectra showed that the helical content remains essentially unchanged over this 50 °C temperature range (55% at 37 °C; 49% at 87 °C).

Two further experiments were carried out to investigate the origin of the band observed at 1633 ± 3 cm^{-1}. First,

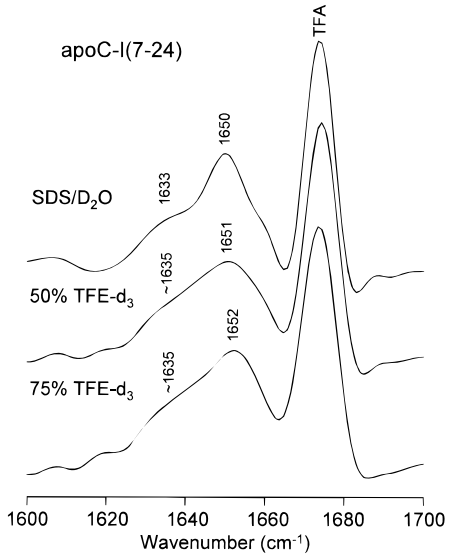

FIGURE 6: Deconvolved infrared absorption spectra for apoC-I(7−24) (10 mg/mL) in mixtures of trifluoroethanol-d_3/D_2O, and in SDS/D_2O. All spectra were deconvolved (half-bandwidth = 16 cm^{-1}, band narrowing factor = 2).

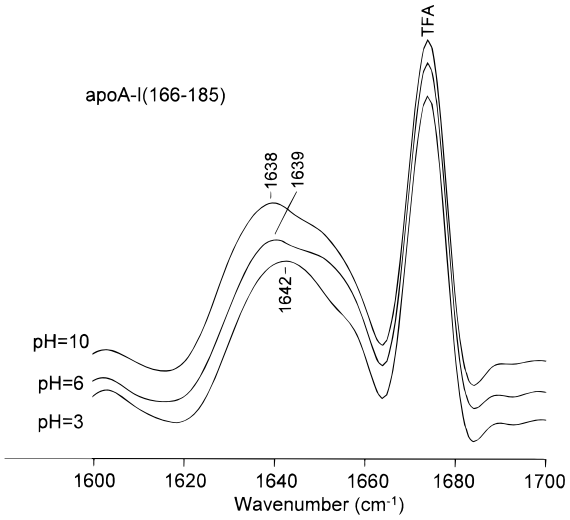

FIGURE 7: Infrared absorption spectra for apoA-I(166−185) in SDS/D_2O solution at pH 3, 6, and 10. All spectra were deconvolved (half-bandwidth = 16 cm^{-1}, band narrowing factor = 2).

spectra were recorded for apoC-I(7−24) in the presence of trifluoroethanol-d_3, a structure-inducing cosolvent (Tamburro et al., 1968; Goodman et al., 1971) that has been previously shown by NMR and CD spectroscopy to promote helix formation in apoC-I(7−24) (Rozek and Cushley, unpublished results). In mixed TFE-d_3/D_2O solvents, apoC-I(7−24) gives rise to absorptions at 1651/1652 cm^{-1} and at *ca.* 1635 cm^{-1} that are evidently analogs of the absorptions observed in SDS/D_2O (see Figure 6). Second, we have studied the pH dependence of the IR spectrum for apoA-I(166−185) in SDS/D_2O. The IR spectra, plotted in Figure 7, show a shift in the absorption maximum to lower frequency with increasing pH that is consistent with a simultaneous decrease in the amount of random coil structure (diminished absorption intensity at 1645 cm^{-1}) and an increase in the structure responsible for the absorption at *ca.* 1636 cm^{-1}.

Although generally considered to act as a spectator ion and not to influence peptide properties, there was some concern that the unusual low-frequency IR absorptions might be due to peptide structures either involving, or uniquely promoted by, the presence of TFA. To exclude such a possibility, the TFA was completely removed from one of the peptides [apoC-I(7−24)]. The deconvolved IR spectra are plotted in Figure 8 for the free peptide in D_2O (upper curve) and in the presence of a 1:40 molar excess of perdeuterated SDS (lower curve). The characteristic low-frequency absorption (1633 cm^{-1}) remains prominent in the latter spectrum, indicating that trifluoroacetate does not influence the secondary structure adopted by the six peptides in SDS/D_2O.

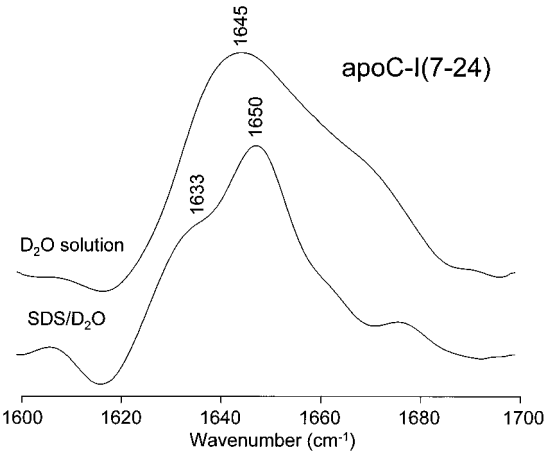

FIGURE 8: Infrared absorption spectra for trifluoroacetate-free apoC-I(7−24) in D_2O solution (upper trace) and in SDS/D_2O (lower trace), deconvolved using half-bandwidth = 16 cm^{-1}, band narrowing factor = 2.

DISCUSSION

Absorptions Below 1640 cm^{-1}: Vibrational Assignments. The assignment for the lowest frequency amide I absorptions is not straightforward. While bands in this region are generally attributed to β-structure, the NMR-derived structures clearly rule out this interpretation. Some guidance may be derived by comparing the absorption patterns for LAP-20, apoA-II(18−30)+, and the two apoC-I fragments (Figure 2). These spectra all show only two well-resolved absorptions, with the band positions and relative intensities approximately equal in all four spectra. The relative intensities are consistent with approximately 80% of the C═O groups participating in helical structure and approximately 20% contributing to a second structural domain that is common to these four peptides. In this context, it is worth highlighting that the three C═O groups adjacent to the C-terminal are by definition excluded from participation in the $i \rightarrow i+4$ hydrogen bonding characteristic of an α-helix (no NH donors exist beyond the end of the peptide). This creates a subset of C═O groups, approximately 13−17% of the total, that would be expected to give rise to an IR absorption removed from that of the helix proper. As a working hypothesis, we therefore assigned the absorptions at 1631−1636 cm^{-1} in all six peptides to the three C═O oscillators at the C-terminus.

The CD spectra are also consistent with predominantly α-helical structures for the six peptides. However, the indications of random coil structure and other components generally attributed to β-pleats and β- and γ-turns (Table 4) are not consistent with the NMR-derived structures or the NMR spectra. Interpretation of the CD spectra and CCA results therefore present challenges that parallel those

encountered for the IR spectra, indications of β- (or β-like) structure where the NMR structure calculations indicate that none exists. Combined with the difficulties in fully assigning the IR spectra, we interpret the CCA results to suggest the presence of an unusual structure that 'masquerades' as β-structure both in the IR and in the CD spectra.

Increasing temperature resulted in either no change or a loss of intensity in the lowest frequency IR absorption (Figure 4), suggesting that the band is associated with an ordered structure. The thermal behavior further suggested a division of the peptides into two groups. The first group includes apoA-II(18−30)+, LAP-20, and the two apoC-I peptides. Although there is generally a transfer of intensity away from the lowest frequency absorption, these changes are minor in comparison to those observed for the peptides in the second group [apoA-I(166−185) and apoE(267−289)], each of which undergoes a marked increase in random coil structure with increasing temperature. The increase in random coil structure observed for apoE(267−289) is clearly at the expense of the absorptions at 1636 and 1654 cm^{-1}. The corresponding absorptions (helix at 1654 cm^{-1}, random coil at 1645 cm^{-1}, and the third absorption at 1636 cm^{-1}) are not as well resolved in the spectra of apoA-I(166−185). However, curve-fitting each of the spectra collected between 15 and 80 °C (Figure 5) confirmed that the increased intensity at 1645 cm^{-1} (random coil) is derived largely at the expense of the absorption at 1636 cm^{-1}, with the intensity of the helix band remaining virtually unchanged. CD spectra collected over the temperature range 37−87 °C confirmed the stability of the apoA-I(166−185) helical structure. The observation of these low-frequency absorptions in TFE-d_3/D_2O solution further confirms that the structure(s) responsible is (are) not promoted uniquely by peptide/SDS interaction.

The IR spectrum of apoA-I(166−185) in SDS/D_2O shows a subtle pH dependence, as illustrated in Figure 7. The NMR spectra at pH 3.7 and 6.6 have been interpreted on the basis of H^{α} secondary shifts to suggest 57% and 71% helical content, respectively (Wang et al., 1996b). In addition, the NMR-derived structure at pH 3.7 lacks two $i \rightarrow i+4$ hydrogen bonds that are present in the corresponding geometry at pH 6.6. The NMR spectrum at pH 10 is essentially identical to that observed at pH 6.6 (Wang and Cushley, unpublished results). The IR spectra measured at pH 3, 7, and 10 (Figure 7) show that increasing pH (and hence the helical content) results in an increase in the structure responsible for the absorption at *ca.* 1636 cm^{-1} and a decrease in the amount of random coil, suggesting that the lowest frequency absorptions may be associated with helical structures. Again, the possibility of self-association contributing to the observed changes in the IR spectra is ruled out by the NMR experiments at pH 3.7, 6.6, and 10, in particular by the line widths (Buchko et al., 1996b) and by absence of NOE's characteristic of self-association.

Absorptions Below 1640 cm^{-1}: Structural Implications. The IR absorption at 1631−1636 cm^{-1} accounts for close to 40% of the total amide I intensity for apoA-I(166−185) and apoE(267−289), and 20% of the total amide I absorption intensity for apoA-II(18−30)+, LAP-20, and the two apoC-I peptides. These intensity values suggest that 2−4 C═O groups for the former four peptides, and approximately 8 C═O groups for the latter two peptides, are included in a region of secondary structure that mimics both the IR and CD spectral signatures characteristic of β-structure.

Anomalous IR amide I absorptions have been reported previously for peptides and proteins that are predominantly α-helical, including bands in low-frequency regions generally associated with β-structure. For example, an early systematic investigation of protein structure using IR spectroscopy revealed absorptions at 1627−1638 cm^{-1} in the spectra of hemoglobin, myoglobin, cytochrome *c*, and ferritin despite the fact that each is known to be almost exclusively α-helical (Byler & Susi, 1986). These bands were attributed to short, extended chains connecting helical cylinders. This interpretation cannot explain the analogous bands observed for the transmembrane peptide Ac-K_2-$(LA)_{12}$-K_2-NH_2, which also shows absorptions at 1633−1637 cm^{-1} in a variety of media despite CD and NMR evidence indicating a predominantly α-helical structure (Zhang et al., 1995). It has also been observed that pattern recognition methods for spectra/structure correlation are more effective if the terminal residues in α-helical domains are treated as entities distinct from the core of the helix (Dousseau & Pézolet, 1990). This requirement was ascribed to decreased order at the termini, and hence to hydrogen bonding patterns that differ substantially from that of the helix core (Van Wart & Scheraga, 1978; Berjot et al., 1987).

These studies are all consistent with the notion that absorptions below 1640 cm^{-1} may be associated with a distorted helical structure. This interpretation is further supported by the increased absorption intensity as the pH (and helical content) of apoA-I(166−185) is raised. An unusual hydrogen bonding pattern would account for the low amide I (C═O stretching) frequency, with either exceptionally strong hydrogen bonds or C═O groups that simultaneously accept two or more H-bonding donor protons. Peptide C═O groups that accept more than one hydrogen bonding donor are not uncommon. For example, a study of 10 protein crystallographic structures has shown that more than 15% of backbone C═O groups form hydrogen bonds simultaneously with water OH and backbone NH groups, the vast majority of these occurring in α-helices (Baker & Hubbard, 1984). Indeed, less than half of the backbone C═O groups are involved in 'textbook' hydrogen bonding patterns, i.e., engaged in only a single hydrogen bond with a backbone NH donor.

There are three possible arrangements that result in a C═O group participating in two hydrogen bonds simultaneously; the donors may be two backbone NH groups, two solvent OH(D) groups, or one of each. For the three C═O groups at the C-terminal, the possibilities are further limited, since there are no NH groups available to participate in $i \rightarrow i+4$ hydrogen bonds characteristic of α-helices. We are therefore led to suggest that these three terminal C═O groups may accept hydrogen bonds simultaneously from two solvent molecules. This mechanism simultaneously explains a number of key observations: the consistent vibrational assignments for the three terminal C═O groups, the similarities among the IR absorption patterns for apoA-II(18−30)+, LAP-20, apoC-I(7−24), and apoC-I(35−53), and the observation that these four IR spectra show no evidence of the random coil structure that would otherwise be expected for the C-termini.

Finally, this proposed mechanism can be extended to account for the relatively high intensity and marginally higher frequency (1636 cm^{-1}) observed for the corresponding absorptions in the IR spectra of apoA-I(166−185) and apoE-

(267−289). We attribute this to the solvent interacting with additional C═O groups along the backbone (i.e., involving C═O groups other than the three closest to the C-terminal), forming bifurcated NH/OH→O═C and/or OH/OH→O═C hydrogen bonds. While these regions may be associated with SDS less intimately than 'normal' helical regions responsible for the absorptions at *ca.* 1655 cm^{-1}, the NMR-derived structures confirm that the helical motif is retained nevertheless. We view these unusual helices as regions wherein the balance between stabilizing hydrophobic interactions with SDS and destabilizing interactions with water (all of the peptides are structureless in aqueous solution) is shifted, resulting in helical regions that remain associated with SDS yet are relatively accessible to the solvent.

Having attributed the absorptions labeled 'other' in Table 3 to distorted helices, the final set of vibrational assignments implies only helical and random coil structures in the SDS-bound peptides. This is consistent not only with the NMR-derived evidence but also with early work demonstrating a clear reduction in apolipoprotein β-structure upon interaction with SDS (Gotto et al., 1968).

Relative Populations and Thermal Stabilities of IR-Determined Secondary Structures. An Indicator of Lipid-Binding Affinities? While IR spectroscopy can occasionally be ambiguous in providing absolute estimates of secondary structure, there is little ambiguity in concluding from the IR spectra alone that the secondary structures are predominantly helical and closely similar for apoA-II(18−30)+, LAP-20, and the two apoC-I peptides in association with SDS. In contrast, the structures of both apoA-I(166−185) and apoE-(267−289) include regions that are disordered to the extent that clear indications of random coil structure emerge in the IR spectra.

The CCA analyses of the CD spectra reflect this distinction in that the fractional α-helical content is lowest for apoE-(267−289) and apoA-I(166−185) (Table 4). However, the estimates of random coil structures are completely inconsistent with those derived from the IR spectra. These discrepancies may be rationalized to a degree by noting that the bases for deriving secondary structure estimates are indirect and are entirely different for the two methods; while IR spectroscopy of the amide I bands monitors the strength of H-bonding to the backbone C═O groups (Jackson & Mantsch, 1991), circular dichroism spectroscopy reflects the dihedral angles (Bloemendal & Johnson, 1995). A detailed discussion of the relative strengths of the two methods is beyond the scope of this paper; however, it is generally considered true that neither method is accurate to better than ±10% in quantitating secondary structures (Surewicz et al., 1993; Bloemendal & Johnson, 1995). The CD results are probably even less accurate for these peptides in association with SDS, due to the presence of structural features that are not modeled in the CCA basis set. The poor performance of the CCA analyses is most evident in those cases where substantial contributions from (nonexistent) β- (or γ-) structures are included in the secondary structure breakdown. However, the secondary structures 'misinterpreted' as β-structures are found in all six peptides, and the accompanying CD signatures are by definition misassigned to other motifs. All of the CCA results summarized in Table 4 are therefore likely to be less reliable than is the case in 'routine' applications, and even under ideal circumstances, the CCA method is poor in quantitating random coil structure (Bloemendal & Johnson, 1995).

In contrast, the unusual low-frequency features in the IR spectra are well separated from those due to helical and random coil structures and therefore do not confound the trends observed in those structures. We therefore consider the results of the IR analyses, summarized in Table 3, to be a better qualitative indicator of similarities and differences among the secondary structures, particularly in singling out apoA-I(166−185) and apoE(267−289) as including regions of random coil structure. One explanation for this disorder may be that the peptide/SDS interaction is relatively weak for apoA-I(166−185) and apoE(267−289) as compared to the other four peptides. This observation is consistent with previous studies of intact apolipoproteins which suggest that the protein/lipid interaction may be weaker for apoA-I and apoE than for apoA-II, apoC-I, and apoC-III. For example, it has been shown that of the four apolipoproteins A-I, A-II, C-I, and C-III, apoA-I binds most weakly to DMPC vesicles (Rosseneau et al., 1976). In addition, it has been suggested that apoC-I may displace apoE from the low-density lipoprotein receptor-related protein (LRP) and block the interaction between apoE-rich β-VLDL and the LRP (Swaney & Weisgraber, 1994).

Independent methods for characterizing amphipathic helices divide the six peptides into two subgroups identical to those suggested by the IR spectra. Various molecular properties such as the charge distribution, the mean hydrophobic moment, and the number/distribution of certain amino acid residues have been analyzed to derive a classification system for the exchangeable lipoproteins and the helical domains contained within them (Segrest et al., 1994); class A amphipathic helices are characterized by clusters of cationic side chains in the interface of the hydrophobic and hydrophilic faces, while for class G* amphipathic helices the cationic side chains are randomly distributed on the hydrophilic face. Class A_2 domains, which are considered to form the best-defined class A amphipathic helices, are further distinguished from class A_1 by a substantially higher mean hydrophobic moment and are distinguished from both class A_1 and class G* by a substantially higher ratio of lysine to arginine.

The two apoC-I peptides, apoA-II(18−30)+, and LAP-20 are all predicted to form class A_2 helices, while apoA-I(166−185) and apoE(267−289) are predicted to form relatively poorly defined class A_1 and class G* helices, respectively (Segrest et al., 1994). NMR structures elucidated for these peptides in association with SDS are essentially consistent with these predictions (Rozek et al., 1995; Buchko et al., 1996a,b; Wang et al., 1996a,b).

There is growing evidence to suggest that lipid-binding affinity is generally higher for class A_2 helical domains than for class A_1 and class G* helical domains (Brasseur et al., 1992; Mishra & Palgunachari, 1996). The indications of random coil structure in the IR spectra (Figure 2) and the marked increase in random coil structure with increasing temperature (Figure 4) observed for apoA-I(166−185) and apoE(267−289) may therefore serve as general indicators of relatively weak peptide/lipid interactions. Consistent with this is an intramolecular H-bonding network that is relatively weak (and hence more readily destabilized) for apoA-I(166−185) and apoE(267−289), as reflected by the absorptions ascribed to helices appearing at somewhat higher frequency

(1655 ± 1 cm^{-1}) than the corresponding bands for the class A_2 helices (1649 ± 1 cm^{-1}).

CONCLUSION

The results of the present study point out that IR and CD spectral techniques provide structural information that complements the detailed structures calculated from NMR data. While the IR and CD spectra are consistent with the previously derived NMR structures, indicating substantial helical content for all of these peptides interacting with SDS/D_2O, the IR spectra have revealed additional structural information primarily through the interpretation of absorptions at unusually low frequency and through the temperature dependence of the spectra.

In particular, the IR spectra suggest a division of the six peptides into two subsets. For one of these subsets, nearly uniform helical structures are indicated together with short regions (2−3 residues) that are involved in unusual hydrogen bonding; these secondary structures remain essentially unaltered by increasing temperature. This subset includes apoA-II(18−30)+, LAP-20, and the two apoC-I peptides.

ApoA-I(166−185) and apoE(267−289) form the second subset, which is distinguished by: (i) diminished relative intensity of the absorption ascribed to helical structure; (ii) additional IR absorptions characteristic of random coil structure, that are paralleled by relatively large RMSD's in the ensembles of NMR structures; (iii) relatively large segments (8−9 residues) that participate in unusual hydrogen bonding arrangements; (iv) an increase in random coil structure with increasing temperature; and (v) an intramolecular hydrogen bonding network that is relatively weak.

These results parallel model-based estimates of the relative lipid-binding affinities, which predict helices of class A_2 to bind lipid most strongly (Segrest et al., 1994). We therefore suggest that the appearance of IR absorptions at positions generally ascribed to random coil structure—as observed for the class A_1 and G* helices studied here—may serve as a general marker of relatively weak lipid-binding affinity, which is further characterized by the appearance of increasing random coil structure with increasing temperature. This parallel would also appear to confirm the interaction with SDS as a good model of amphipathic helix/lipid interactions.

These conclusions rest partially upon the vibrational assignment for the lowest frequency absorption observed in all the IR spectra. Normally signaling β-structure, this absorption is attributed here to the formation of bifurcated hydrogen bonds in which individual C═O groups act as acceptors for both a solvent OH(D) and either a second solvent donor or a backbone NH(D). The observation that these absorptions also appear for spectra measured in a helicogenic solvent (trifluoroethanol), combined with literature reports of low-frequency absorptions for proteins that are almost exclusively α-helical, suggests that absorptions below 1640 cm^{-1} may be a general feature of helices that include regions that are solvent-accessible.

ACKNOWLEDGMENT

We thank Jim Sparrow (Department of Medicine, Baylor College of Medicine, Houston, TX) for suggesting the method used to remove trifluoroacetate ion from apoC-I(7−24).

REFERENCES

Assmann, G., & Brewer, H. B. (1974) *Proc. Natl. Acad. Sci. U.S.A. 71*, 1534−1538.
Atkinson, D., & Small, D. M. (1986) *Annu. Rev. Biophys. Biophys. Chem. 15*, 403−456.
Baker, E. N., & Hubbard, R. E. (1984) *Prog. Biophys. Mol. Biol. 44*, 97−179.
Bax, A., & Davis, D. G. (1985) *J. Magn. Reson. 65*, 355−360.
Berjot, M., Marx, J., & Alix, A. J. P. (1987) *J. Raman Spectrosc. 18*, 289−300.
Bloemendal, M., & Johnson, Jr. (1995) *Pharm. Biotechnol. 7*, 65−100.
Brasseur, R., Lins, L., Vanloo, B., Ruysschaert, J.-M., & Rosseneau, M. (1992) *Proteins: Struct., Funct., Genet. 13*, 246−257.
Braunschweiler, L., & Ernst, R. R. (1983) *J. Magn. Reson. 53*, 521−528.
Buchko, G. W., Treleaven, W. D., Dunne, S. J., Tracey, A. S., & Cushley, R. J. (1996a) *J. Biol. Chem. 271*, 3039−3045.
Buchko, G. W., Wang, G., Pierens, G. K., & Cushley, R. J. (1996b) *Int. J. Pept. Protein Res. 48*, 21−30.
Byler, D. M., & Susi, H. (1986) *Biopolymers 25*, 469−487.
Clark-Lewis, I., Aebersold, R. A., Ziltner, H., Schrader, J. W., Hood, L. A., & Kent, S. B. H. (1986) *Science 231*, 134−139.
Dolphin, P. J. (1985) *Can. J. Biochem. Cell Biol. 63*, 840−869.
Dousseau, F., & Pézolet, M. (1990) *Biochemistry 29*, 8771−8779.
Goodman, M., Naider, F., & Toniolo, C. (1971) *Biopolymers 10*, 1719−1730.
Gotto, A. M., Levy R. I., & Fredrickson D. S. (1968) *Proc. Natl. Acad. Sci. U.S.A. 60*, 1436−1441.
Jackson, M., & Mantsch, H. H. (1991) *Can. J. Chem. 69*, 1639−1642.
Lusis, A. J. (1988) *J. Lipid Res. 29*, 397−429.
Mahley, R. W. (1988) *Science 240*, 622−630.
Miller, G. J., & Miller, N. E. (1975) *Lancet 1*, 16−19.
Mishra, V. K., & Palgunachari, M. N. (1996) *Biochemistry 35*, 11210−11220.
Perczel, A., Park, K., & Fasman, G. D. (1992) *Anal. Biochem. 203*, 83−93.
Pownall, H. J., Hu, A., Gotto, A. M., Albers, J. J., & Sparrow, J. T. (1980) *Proc. Natl. Acad. Sci. U.S.A. 77*, 3154−3158.
Rosseneau, M., Soetewey, F., Blaton, V., Lievens, J., & Peeters, H. (1976) *Chem. Phys. Lipids 17*, 38−56.
Rozek, A., Buchko, G. W., & Cushley, R. J. (1995) *Biochemistry 34*, 7401−7408.
Ryan, R. O. (1996) *Biochem. Cell Biol. 74*, 155−164.
Segrest, J. P., Jackson, R. I., Morrisett, J. D., & Gotto, A. M., Jr. (1974) *FEBS Lett. 38*, 247−253.
Segrest, J. P., Garber, D. W., Brouillette, C. G., Harvey, S. C., & Anantharamaiah, G. M. (1994) *Adv. Protein Chem. 45*, 303−369.
Shen, B. W., Seanu, A. M., & Kezdy, F. J. (1977) *Proc. Natl. Acad. Sci. U.S.A. 74*, 837−841.
Surewicz, W. K., & Mantsch, H. H. (1988) *Biochim. Biophys. Acta 952*, 115−130.
Surewicz, W. K., Mantsch, H. H., & Chapman, D. (1993) *Biochemistry 32*, 389−394.
Swaney, J. B., & Weisgraber, K. H. (1994) *J. Lipid Res. 35*, 134−142.
Tamburro, A. M., Scatturin, A., Rocchi, R., Marchiori, F., Borin, G., & Scoffone, E. (1968) *FEBS Lett. 1*, 298−300.
Van Wart, H. E., & Scheraga, H. A. (1978) *Methods Enzymol. 49*, 67−149.
Wang, G., Pierens, G. K., Treleaven, W. D., Sparrow, J. T., & Cushley, R. J. (1996a) *Biochemistry 35*, 10358−10366.
Wang, G., Treleaven, W. D., & Cushley, R. J. (1996b) *Biochim. Biophys. Acta 1301*, 174−184.
Zhang, Y.-P., Lewis, R. N. A. H., Henry, G. D., Sykes, B. D., Hodges, R. S., & McElhaney, R. N. (1995) *Biochemistry 34*, 2348−2361.

BI970558S